

ISOTHERMAL CRYSTALLIZATION OF Cu₂ZnSnS₄ IN MOLTEN NaI, STARTING FROM FRESHLY SYNTHESIZED CuS AND SnS₂

H. M. KAMKUI^{a,*}, A. T. DJOWE^a, S. LAMINSI^a, D. NJOPWOUO^b

^aLaboratory of Physical Chemistry and Applied Analytical Chemistry Department of Inorganic Chemistry, Faculty of Sciences, University of Yaoundé I, P.O Box 812 Yaoundé, Cameroon

^bLaboratory of Applied Inorganic Chemistry, Department of Inorganic Chemistry, Faculty of Sciences, University of Yaoundé I, P.O Box 812 Yaoundé, Cameroon

This paper reports the study of the isothermal crystallization of Cu₂ZnSnS₄ in sodium iodide at 680°C, 750°C and 800°C. CuS is obtained by hydrothermal synthesis at 100°C. The products of reactions were characterized using XRD, XRF, TDA and TGA. The TDA and TGA thermograms of synthesized CuS show the main thermal transformations described in the literature, but some particularities as concerning the thermal reactions temperatures were observed. The diameters of CuS crystallites are between 38.53 nm and 41.51 nm. Synthesized CuS is transformed into Cu₂S at 345°C. At 680°C, the product of isothermal crystallization in NaI is formed of three crystalline phases: sphalerite, anillite and kesterite. At 750°C, we obtain a mixture of three crystalline phases: sphalerite, herzenbergite and kesterite. At 800°C, the isothermal crystallization product consists of a single crystalline phase: kesterite. The formed kesterite is rich in copper and tin while its amount in sulfur and zinc is low. The diffusion rate of the reactants increases with temperature and reaches an optimum value at 800°C.

(Received September 16, 2018; Accepted November 20, 2018)

Keywords: Sodium iodide, Isothermal crystallization, Hydrothermal synthesis, Covellite (CuS), Kestérite (Cu₂ZnSnS₄)

1. Introduction

Binary and quaternary Sulfides have been given in recent years a renewed interest because of their exceptional electrical properties [1-4]. Binary sulfides of transition metals have also proven a special interest in the field of catalysis [5,6]. With the advent of quaternary chalcogenides in the field of solar energy, binary sulfides of transition metals were used as precursors for the synthesis of quaternary chalcogenides [7-9]. Cu₂ZnSnS₄ usually named CZTS is a quaternary chalcogenide used as absorbent in solar cells and therefore renewed interest in these two decades.

CZTS is a p-type semiconductor with an absorption coefficient of 10⁴cm⁻¹ [10] with an energy gap of 1.5 eV [11-13]. Several techniques for synthesizing CZTS have been explored [14-17]. Among them, the synthesis of CZTS monograins in a molten salt has the advantage of producing layers of monograins from a material known and characterized in advance. Timmo et al. studied the synthesis of CZTS in potassium iodide melted at 1000K and noted the presence of several secondary phases, however, KCN leaching allows the remove of some secondary phases[16].

The formation and growth of CZTS monograins in CdI₂ has recently been studied. CZTS begins to form in CdI₂ at 370°C, just below the melting point of CdI₂ (387°C). Secondary phases still appear and the possible incorporation of Cd in the CZTS matrix [18].

Molten salts have proven their effectiveness as a reaction medium for the formation and growth of CZTS monograins, however, the secondary phases that form depend on the crystallization temperature and the precursors [16, 18, 19]. The granulometry and morphology of precursors influence the formation and growth of crystals in a molten salt, were the diffusion of reactants is the process by which precursors combine.

* Corresponding author: mossakhilaire@yahoo.fr

The formation of CZTSe in NaI has already been the subject of a preliminary study and it has been shown that CZTSe forms from 380°C [20]. Here, we report for the first time the crystallization of CZTS in molten NaI, at temperatures 680°C, 750°C and 800°C starting from freshly synthesized SnS₂ microplates and CuS. At each of these temperatures, we have identified the secondary crystallines formed phases.

2. Experimental

2.1 Reagents

Hydrochloric acid (37%), sulfur (99%), methanol (99.8%), tin sulphate (98%) sodium hydroxide(99%), carbon disulphide (99%) zinc sulfide (99%) were purchased from Riedel-de Haen and used without any treatment.

Copper powder (97%) was purchased from Gundong Chemical Reagent. According to the manufacturer, this powder was obtained by precipitation. Unfortunately, the precipitation technique has disadvantage of producing metal powders containing enough impurities. The pristine copper powder was washed with concentrated hydrochloric acid, consequently rinsed with distilled water and dried in air for two hours before use. This operation was done in order to remove some of impurities.

2.2 Synthesis

We reported the synthesis and characterization of tin disulfide microplates elsewhere [21]. CuS is synthesized using a method derived from that described by Tezuka et al. [22]. Briefly, 0.03 mole of sulfur and 0.03 mole of copper powder were intimately mixed in a porcelain mortar and transferred into a 50 mL stainless steel mini-autoclave containing 20 mL of distilled water. The mini-autoclave was heated at 100°C for 24 hours and then, cooled at room temperature. The obtained product was successively washed with carbon disulfide and methanol before being rinsed with distilled water. The resulting powder was dried in an oven at 100°C until constant weight and kept away from air and moisture. During the drying process, a slight color change of the product was observed, suggesting that the reaction between copper and sulfur still continues. The final color or the product was indigo-blue, which is the well-known color of covellite.

Obtained Copper sulfide was preheated at 345°C for ten minutes, after cooling at room temperature it was intimately mixed with Tin disulfide and zinc sulfide in porcelain mortar. The masses of the reactants are such as: Cu: Zn: Sn: S is equal to 2: 1: 1: 4. Sodium iodide was added to the mixture, to a volume nearly equal to the volume of the mixture of binary sulphides, in order to facilitate the diffusion of reactants [23]. The mixture was homogenized and dried in an oven at 100°C for 24 hours. After drying, the mixture was grinded, introduced into a quartz glass tube and sealed under vacuum. The mixture was Heated to the desired temperature at the heating rate of 10°C per minute up to 380°C and then, at 1°C per minute from 380°C to 450°C and 10°C per minute from 450°C to the final temperature. The oven was kept at the final temperature for 72 hours. The quartz glass tube was removed from the oven, quenched in melting ice, broken and the product was recovered by dissolving and washing it in distilled water. The product was dried in an oven until constant weight.

2.3 Characterization

X-ray powder diffraction (XRD) data were collected at room temperature with a Siemens D 5000 diffractometer operating with the focusing Bragg-Brentano geometry, using Cu-K α radiation ($\lambda=1.5406 \text{ \AA}$). The diffraction patterns were collected at 40 kV and 40 mA over the angular range 2°-70° (2 θ) with a counting time of 1s/step and a step length of 0.02° (2 θ). Another X-ray diffraction (XRD) data were collected at room temperature with a D8 Bruker advance diffractometer operating with the focusing Bragg-Brentano geometry, using Cu-K α radiation ($\lambda=1.5406 \text{ \AA}$). The diffraction patterns were collected at 40 kV and 40 mA, over the angular range of 5°- 60° (2 θ) with a counting time of 10s/step and a step length of 0.02°(2 θ). Elemental analyses were carried out using a WDX-Ray fluorescence spectrometer (S4 Pioneer, Bruker). The TGA-DTA measurements of the samples were done with a thermal analyzer (TA Instruments, Model

STD 2960, simultaneous DTA-TGA) at a heating rate of $10^{\circ}\text{C}.\text{min}^{-1}$ in an air atmosphere, starting at room temperature with sample mass of about 66 mg for CuS and 86.5 mg for $\text{Cu}_2\text{ZnSnS}_4$ obtained at 750°C .

3. Results and discussion

3.1 XRF, XRD characterizations and thermal analysis of the synthesized covellite (CuS)

Chemical composition of synthesized covellite (CuS) is presented in Table 1.

Table 1. Chemical composition of as synthesized CuS.

Elements	ppm
Cu	$49,5 \times 10^4$
S	$49,0 \times 10^4$

The XRF elemental analysis performed on synthesized CuS revealed that; copper and sulfur are present in ratio Cu:S = 1.01:1 confirming the formation of stoichiometric CuS.

The XRD pattern of the synthesized material was depicted on Fig. 1. This figure shows diffraction peaks that index the hexagonal phase of CuS (ASTM 78-877 Space Group: P63/mmc; $a = 3.7938$; $c = 16.3410$; $Z = 6$) indicating that the synthesized product is crystalline. Since the experimental lattice constants determined in this case were $a = 3.7900\text{\AA}$ and $c = 16.3404\text{\AA}$, we found $c/a = 4.3110$. These values are close to standard values.

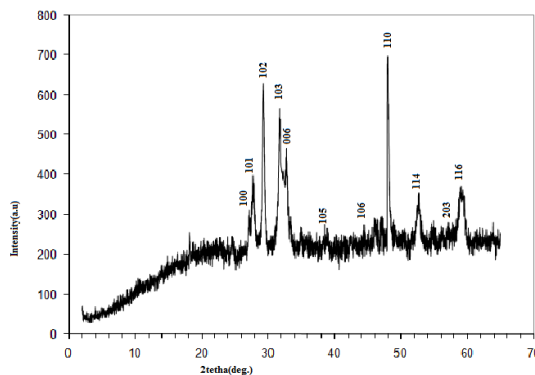


Fig. 1 XRD pattern of CuS obtained by hydrothermal synthesis from copper and sulfur at 100°C .

It was shown that the hydrothermally synthesized CuS obtained after corrosion process between copper and sulfur has spherical-closed polyhedral particles [22]. For this reason, crystallite diameter can be determined by Scherrer formula. $D = 0.91\lambda/\beta\cos\theta$ (1)

Where, λ represents the wavelength of Cu-K α radiation (1.5406\AA), D the crystallite diameter and β the full width at half maximum (FWHM) of covellite reflection corresponding to the XRD reflection angles 2θ . The crystallites diameter determined for each reflection peak is presented in Table 2.

Table 2. Crystallite diameter of CuS hydrothermally synthesized (calculations based on the FWHM

data of the reflection at $2\theta = 28; 29.4; 32; 48$ and 52.8 .

2θ (deg)	28.0	29.4	32.0	48.0	52.8
FWHM $\times 10^3$ (rad)	3.75	3,73	2,98	4,01	3,77
D (nm)	38,53	38,85	48,94	38,26	41,51

The average value of the diameter of the crystallites is $D_{moy} = 41.22$ nm. Blachnik and Muller observed that, below 165°C , CuS obtained by hydrothermal corrosion of copper with sulfur retained the grain shape and size of the copper powder [24]. C.M. Simonescu and coworkers have brought out that, the shape of the X-ray diffraction pattern depended on the proportion of the starting reagents, getting covellite from copper acetate and sodium thiosulfate [25]. These observations show that, the particle size of the starting reagents affects the crystallinity of synthesized CuS and may affect its thermal oxidation in air.

Fig. 2 presents the TGA and DTA curve of the hydrothermally synthesized covellite. It can be deduced from this figure that the transformations occurring during thermal treatment of covellite in air can be summarized into four main steps described as follow:

- (i) formation of a lower sulfur content sulfide,
- (ii) oxidation of the sulfide formed,
- (iii) formation of the copper oxysulfate,
- (iv) decomposition of copper oxysulfate.

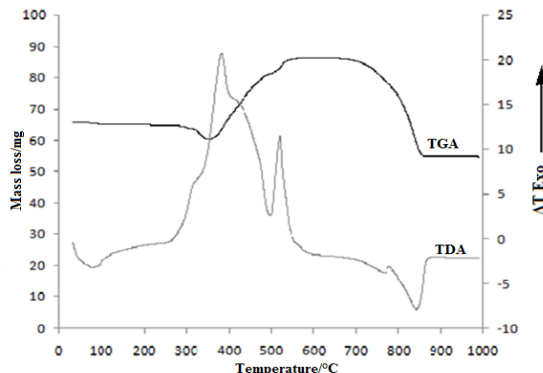
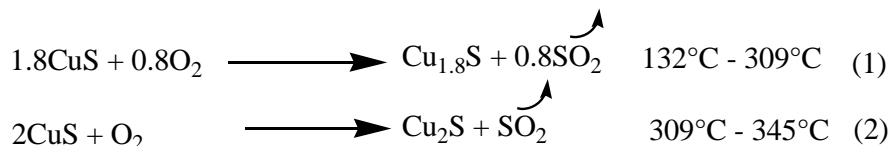


Fig. 2. TGA and DTA curves of CuS hydrothermally obtained from copper and sulfur.

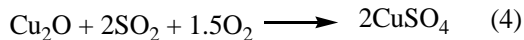
The thermal decomposition of CuS with crystallite size between 38.53 nm and 41.51 nm starts with a small gradual mass loss from 34°C to 309°C ($\Delta m = -5$ mg). This loss of mass is done in two stages: between 34°C and 132°C we observed the elimination of adsorbed water ($\Delta m = -1.25$ mg). The formation of digenite ($\text{Cu}_{1.8}\text{S}$) and chalcocite (Cu_2S) begins from 132°C until 309°C [26,27].

From 309°C to 345°C the loss of mass becomes more significant and was mainly due to the formation of Cu_2S . The main reactions that occur are represented by equations (1) and (2).



The next process ($346^\circ\text{C} - 545^\circ\text{C}$) was performed in two steps with a mass gain ($\Delta m = +30$ mg). Several phases have been identified in this temperature range: $\text{Cu}_{1.8}\text{S}$; Cu_2S ; Cu_2O ; CuO ; CuSO_4 and CuO.CuSO_4 [26,27]. Such mass gain was attributed to the formation of CuSO_4 .

up to 482°C and that of CuO.CuSO₄ from 482°C to 545°C. The main reactions can be described by equations (3), (4) and (5).



The plateau observed between 545 °C and 667 °C reflects the thermal stability of the formed copper oxysulfate. Between 667°C and 832°C the TGA curve shows a significant loss of mass ($\Delta m = -33$ mg) owing to the decomposition of copper oxysulfate to form copper (II) oxide, according to equation (6).



The TGA curve presents a second plateau between 845°C and 961°C that explains the thermal stability of CuO in this temperature range.

The DTA curve of Fig. 2 shows six thermal characteristic pics:

- 1- An endothermic hook culminating at $T_{\max,\text{TDA}} = 73^\circ\text{C}$.
- 2- A shoulder at 309°C
- 3- A high amplitude exothermic peak at $T_{\max,\text{TDA}} = 377^\circ\text{C}$
- 4- A shoulder at 425°C
- 5- A high amplitude exothermic peak culminating at $T_{\max,\text{TDA}} = 520^\circ\text{C}$.
- 6- An endothermic hook at $T_{\max,\text{TDA}} = 845^\circ\text{C}$.

The endothermic hook observed between 34°C and 136°C and which reaches its maximum at 73°C confirms the elimination of adsorbed water. The formation of digenite and chalcocite is followed by oxidation of sulfur, which subsequently combines with oxygen. The oxidation of sulphur is an exothermic reaction, hence the high amplitude exothermic peak culminating at $T_{\max,\text{TDA}} = 377^\circ\text{C}$. The evolution of this peak hides two others exothermic peaks, which explains the shoulders observed at 309°C and 425°C. Between 309°C and 346°C, the oxidation of sulfur is performed in two stages. The formation of Cu₂O is also followed by oxidation of sulfur, hence, the peak at $T_{\max,\text{TDA}} = 377^\circ\text{C}$ was very intense and extends beyond 346°C. The exothermic shoulder observed at 425°C reflects on the one hand the oxidation of Cu (I) in Cu (II) while on the other hand it suggest the oxidation of S (-II) into S (+VI) followed by formation of SO₄²⁻. The exothermic oxidation of Cu(I) to Cu(II) explains the exothermic peak culminating at 520°C and the faster formation of CuO.CuSO₄ explains the change of pace of the TGA curve.

The endothermic hook at $T_{\max,\text{TDA}} = 845^\circ\text{C}$ reflects the reduction of sulfur (+VI) to sulfur (+IV) during the decomposition of CuO.CuSO₄, followed by the formation of CuO, SO₂ and O₂.

3.2 XRD characterization of product obtained after isothermal crystallization at 680°C

The XRD pattern of the product obtained after isothermal crystallization at 680°C is depicted on Fig. 3.

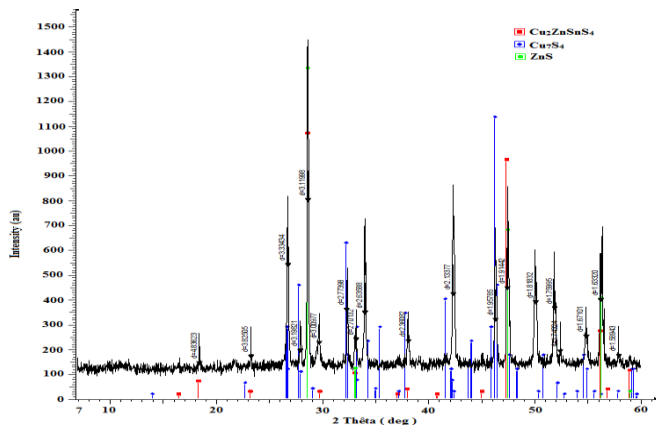


Fig. 3. XRD pattern of the product obtained after isothermal crystallization at 680°C.

The product obtained at 680°C is a mixture of three crystalline phases. The XRD pattern of Fig. 3 shows diffraction peaks that index anillite (ASTM 72-617), sphalerite (JCPDS 5-0566) and kesterite (JCPDS 26-0575).

At 680°C, kesterite ($\text{Cu}_2\text{ZnSnS}_4$) was already formed but sphalerite (ZnS) remains in the product. Anillite (Cu_7S_4) was formed following the reaction between chalcocite (Cu_2S) and digenite ($\text{Cu}_{1.8}\text{S}$). A rise in crystallization temperature could increase the rate of diffusion of the reactants and allows a complete reaction of the binaries.

3.3 XRD characterization and thermal analyses of product obtained after isothermal crystallization at 750°C

The XRD pattern of the product obtained after isothermal crystallization at 750°C was depicted on Fig. 4. The product obtained at 750°C was a mixture of three crystalline phases. The XRD pattern shows diffraction peaks that index herzenbergite (JCPDS 39-354), sphalérite and kestérite. We observed the disappearance of anillite and the formation of herzenbergite.

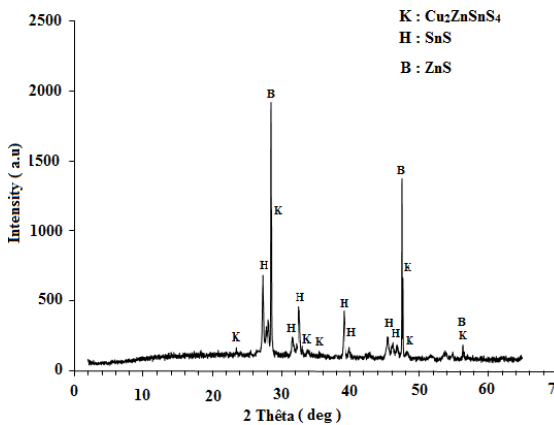


Fig. 4. XRD pattern of the product obtained after isothermal crystallization at 750°C.

The coexistence of kesterite and herzenbergite has already been observed. The work of Weber et al. reports the decomposition of SnS_2 into SnS and S to facilitate the incorporation of ZnS [28].

Fig. 5 presents the TGA and DTA curve of the product obtained after isothermal crystallization at 750°C. The thermal behavior of CZTS under oxygen atmosphere has not yet been the subject of a particular study.

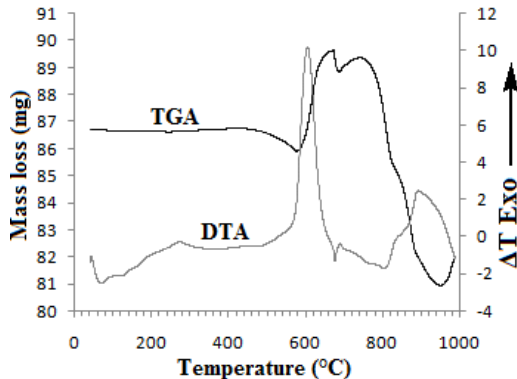
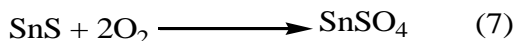


Fig. 5. TGA and DTA curve of the product obtained after isothermal crystallization at 750°C.

From ambient temperature to 440°C, the TGA curve presents a horizontal part, due to the constancy of the mass. From 440°C to 580°C, we observe a slight loss of mass ($\Delta m = -1$ mg). This loss of mass is due to a surface oxidation of SnS into SnO. Under the temperature gradient, this oxidation is increased and reaches its limit around 500°C [29] whence the significant loss of mass observed between 440°C and 580°C. Between 580°C and 680°C, the TGA curve shows a large increase in mass ($\Delta m = + 3.75$ mg). Thermodynamic calculations can predict the reaction among the most plausible is presented by equation (7) [30].



This exothermic reaction explains the mass gain observed from 580°C to 680°C.

The mass loss observed between 680°C and 700°C corresponds to the transformation of sphalerite to zincite (ZnO) according to equation (8) [31].



Between 700°C and 750°C, we observe a slight gain in mass ($\Delta m = + 0.5$ mg). We attribute this mass gain to the formation of SnO₂.

The significant mass loss ($\Delta m = - 8.25$ mg) that occurs between 750°C and 940°C was due to the formation of SnO after the decomposition of SnSO₄. At 840°C we observed the formation of SnO₂, which immediately decomposes into SnO according to the inflection observed at this temperature. The slight weight gain observed between 940°C and 980°C may be due to the possible formation of SnO₂.

The TDA curve of Fig. 5 depicted ten visible thermal phenomena. The endothermic hook which culminates at 70°C confirms the élimination of adsorbed water. The low amplitude endothermic hooks observed at $T_{\max, \text{ATD}} = 125^\circ\text{C}$ and $T_{\max, \text{ATD}} = 160^\circ\text{C}$, can be explained by the formation of small amount of SnO followed by the production of liquid sulfur [30]. Around 270°C, liquid sulfur combines with oxygen as indicated by the exothermic peak at $T_{\max, \text{ATD}} = 270^\circ\text{C}$. The formation of tin sulfate is preceded by the oxidation of sulfur S (+ II) to S (+ VI), and can explain the high amplitude of exothermic peak at $T_{\max, \text{ATD}} = 600^\circ\text{C}$. The oxidation of sulphur during the transformation of sphalerite (ZnS) into zincite (ZnO) with release of SO₂ explains the exothermic peak culminating at $T_{\max, \text{ATD}} = 690^\circ\text{C}$.

The endothermic peaks at $T_{\max, \text{ATD}} = 760^\circ\text{C}$ and $T_{\max, \text{ATD}} = 805^\circ\text{C}$, given their very low amplitudes and their absence in the literature consulted, can be considered as artifacts. The shoulder observed at 840°C corresponds to the oxidation of Sn (+II) to Sn (+IV) during SnO₂ formation. This oxidation continues up to 880°C, hence the exothermic peak at $T_{\max, \text{ATD}} = 880^\circ\text{C}$. At 775°C and 850°C we do not observe any thermal accident indicating the presence of CTS (Cu₂SnS₃) [32, 33]. CZTS melting can not be clearly observed due to the final analysis temperature of 1000°C. Indeed CZTS melts at 991°C [31].

3.4 XRD and XRF characterization of product obtained after isothermal crystallization at 800°C

The XRD pattern of the product obtained after isothermal crystallization at 800°C is depicted on Fig. 6. The pattern shows diffraction peaks that index kesterite ($\text{Cu}_2\text{ZnSnS}_4$). Crystals grow preferentially along the reticular plane (112). The reticular plan (103) has a relative intensity much higher than the standard value (2.2%): a large number of crystallites are oriented according to this plan.

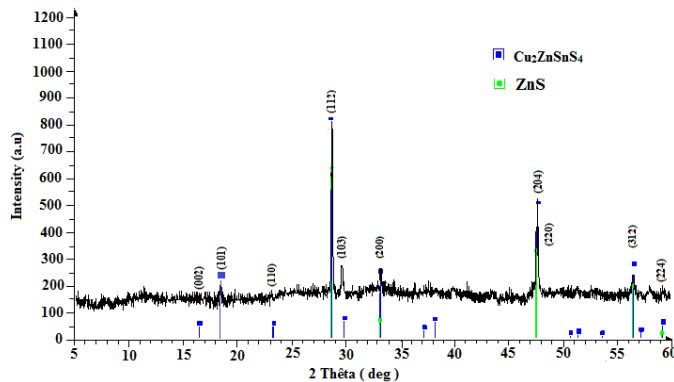


Fig. 6. XRD pattern of the product obtained after isothermal crystallization at 800°C.

At 800°C tin sulfide and copper sulfide reacted completely. None of these binaries do not appear in the crystalline phase: at this temperature, the rate of diffusion of reactants is sufficient to allow their total incorporation into a CTS matrix which is formed at the beginning of reaction. Fig.6, shows diffraction peaks that exclusively index kesterite but the most intense diffraction peaks also index sphalerite. At 800°C we are certain to have synthesized CZTS in molten sodium iodide but we can systematically exclude the presence of sphalerite, due to the limitations of XRD pattern analyses.

Chemical composition of the product obtained after isothermal crystallization at 800°C is presented in Table 3.

Table 3. Chemical composition of product obtained after isothermal crystallization at 800°C.

Elements	Wt %	Stœchiométrie
Cu	27,08	25,00
Zn	10,06	12,50
Sn	12,86	12,50
S	45,00	50,00
I	2,15	0,00
P	0,18	0,00
Ca	0,06	0,00
Undetected	2,61	0,00

Chemical analyses reveal the presence of impurities such as iodine, phosphorus and calcium. The undetermined represent 2.61%. The impurities are found in an amorphous phase that precipitates during cooling. The material obtained was rich in copper and tin and low in sulphur and zinc.

4. Conclusions

We have studied the isothermal crystallization of $\text{Cu}_2\text{ZnSnS}_4$ in NaI at 680°C, 750°C and 800 °C from freshly synthesized covellite (CuS) and berndtite (SnS_2). The product of isothermal crystallization at 680°C consists of three crystalline phases: anillite, sphalerite and kesterite. At 750°C the isothermal crystallization product was also formed of three crystalline phases: sphalerite, herzenbergite and kesterite. At 800°C the only one crystalline phase identified was kesterite. XRD alone, does not allow us to exclude systematically the presence of sphalerite. The diffusion rate of the reactants increases with temperature and reaches an optimum value at 800°C, allowing almost total incorporation of ZnS into a previously formed CTS matrix.

Acknowledgements

The authors gratefully thank the Local materials promotion authority (MIPROMALO) for the XRF and XRD analyses.

References

- [1] S. S. Hegde, A. G. Kunjomana, K. Ramesh, K. A. Chandrasekharan, M. Prashantha, IJSCE, **1**(3), 38 (2011).
- [2] H. Xiao, Y. C. Zhang, H. X. Bai, Mater Lett. **63**(9), 809 (2009).
- [3] M. O. Abou-Helal, M. Boshta, J. Am. Sci. **8**(8), 61(2012).
- [4] J. Cardoso, O. G. Daza, L. Ixtlilco, M. T. S. Nair, P. K. Nair, SEMIC SCI T. **16**(2), 123 (2001).
- [5] Y. C. Zhang, Z. N. Dua, S.Y. Li, M. Zhang, Appl. Catal. B: Environ. **95** (1-2), 153 (2010).
- [6] J. V. Tolia, M. Chakraborty, Z. V. P. Murthy, Pol. J. Chem. Tech. **14**(2), 16 (2012).
- [7] I. Klavina, T. Kaljuvee, K. Timmo, J. Raudoja, R. Traksmaa, M. Altosaar, D. Meissner, Thin Solid Films **519**(21), 7399 (2011).
- [8] B. Su, K. L. Choy, Thin Solid Films **361**, 102 (2000).
- [9] M. Danilson, M. Altosaar, M. Kauk, A. Katerski, J. Krustok, J. Raudoja, Thin Solid Films **519**(21), 7407 (2011).
- [10] K. Ito, T. Nakazawa, Japanese journal of applied physics **27**(11), 2094 (1988).
- [11] A. V. Moholkar, S. S. Shinde, A. R. Babar, K. Sim, H. K. Lee, K. Y. Rajpure, P. S. Patil, C. H. Bhosale, J. H. Kim, Journal of Alloys and Compounds **509**(27), 7439 (2011).
- [12] Z. Zhou , Y. Wang, D. Xu, Y. Zhang, Solar Energy Materials & Solar Cells **94**(12), 2042 (2010).
- [13] A. V. Moholkar, S. S. Shinde, A. R. Babar, K.-U. Sim, H. K. Lee, K. Y. Rajpure, P. S. Patil, C. H. Bhosale, J. H. Kim, Solar Energy **85**(7), 1354 (2011).
- [14] M. L. Liu, F. Q. Huang, L. D. Chen, I. W. Chen, Applied physics letter **94**, 202103 (2009).
- [15] T. Kameyama, T. Osaki, K. I Okazaki, T. Shibayama, A. Kudo, S. Kuwabata, T. Torimoto, Journal of Materials Chemistry **20**, 5319 (2010).
- [16] K. Timmo, M. Altosaar, J. Raudoja, K. Muska, M. Pilvet, M. Kauk, T. Varema, M. Danilson, O. Volobujeva, E. Mellikov, Solar Energy Materials & Solar Cells **94**(11), 1889 (2010).
- [17] J. Zhang, L. Shao, Y. Fu, E. Xie, Rare Met **25**, 315 (2006).
- [18] G. S. C. Chimezie Nkwusi, Formation and growth of $\text{Cu}_2\text{ZnSnS}_4$ monograins powder in molten CdI_2 , Ph.D thesis,Tallinn University of technology, Estonia, June 2017.
- [19] G. Nkwusi, I. Lienemann, J. Raudoja, V. Karber, M. Altosaar, Superlattices and Microstructures **98**, 400 (2016).
- [20] I. Leinemann, J. Raudoja, M. Grossberg, M. Altosaar, D. Meissner, R. Traksmaa, T. Kaljuvee, CYSENI, 2011, Lithuania, conference paper.
- [21] H. Mossak Kamkui, S. Laminsi, D. Njopwouo, A. Tiya Djowe, Chalcogenide letters **11**(5), 219 (2014).

- [22] K. Tezuka, C. W. Sheets, R. Kurihara, Y. Jin Shan, H. Imoto, J. T. Marks, R. K. Poeppelmeier, *Solid State Sciences* **9**(1), 95 (2007).
- [23] E. Mellikov, M. Altosaar, M. Krunks, J. Krustok, T. Varema, O. Volobujeva, M. Grossberg, L. Kaupmees, T. Dedova, K. Timmo, K. Ernits, J. Kois, I. Oja Acik, M. Danilson, S. Bereznev, *Thin Solid Films* **516**, 7125 (2008).
- [24] R. Blachnik, A. Müller, *Thermochimica Acta* **361**(1-2), 31 (2000).
- [25] C. M. Simionescu, V. S. Teodorescu, O. Carp, L. Patron, C. Capatina, *J. Therm. Anal. Calorim.* **88**(1), 71 (2007).
- [26] S. E. Khalafalla, I. D. Shah, *Metallurgical and materials transactions B* **1**, 2151 (1970).
- [27] J. G. Dunn, C. Muzenda, *Thermochimica Acta* **369**(1-2), 117 (2001).
- [28] A. Weber, R. Mainz, T. Unold, S. Schorr, H. W. Schock, *Physica status solidi C* **6**, 1245 (2009).
- [29] A. de Kergommeaux, J. Faure-Vincent, A. Pron, R. de Bettignies, B. Malaman, P. Reiss, *J. Am. Chem. Soc.* **134**(28), 11659 (2012).
- [30] L. A. Burton, Phase stability and composition of tin sulfide for thin-film solar cells, These de doctorat Ph. D, Université de Bath, Angleterre, 2014.
- [31] P. Balaz, J. Huhn, H. Heegn, *Thermochimica Acta* **194**, 189(1992).
- [32] S. Fiechter, M. Martinez, G. Schmidt, W. Henrion, Y. Tomm, *J. Phys. Chem. Solids* **64**(9-10), 1859 (2003).
- [33] G. H. Moh, *Chemie der erde* **34**(1), 1(1975).